Turkish Journal of Electrical Engineering & Computer Sciences

http://journals.tubitak.gov.tr/elektrik/

Research Article

Turk J Elec Eng & Comp Sci
(2020) 28: 1776 – 1790

doi:10.3906/elk-1906-170

Plane wave diffraction by strip with an integral boundary condition

Kamil KARAÇUHA[1,*], **Vasil TABATADZE**[1], **Eldar Ismailovich VELIEV**[1,2]
[1]Informatics Institute, İstanbul Technical University, İstanbul, Turkey
[2]National Technical University, Kharkiv Polytechnic Institute, Kharkiv, Ukraine

Received: 26.06.2019 • **Accepted/Published Online:** 15.11.2019 • **Final Version:** 08.05.2020

Abstract: In this article, a new solution method is proposed for plane wave diffraction by a strip. On the surface of the strip, an integral boundary condition is used. The impedance of the strip is investigated. The theoretical and numerical analyses show that there is a relation between the complex-valued fractional order of the integral boundary condition and properties of the material such as the impedance. As a further study, the total radar cross-section is investigated using the proposed method.

Key words: Electromagnetic diffraction, fractional boundary condition, fractional strip, fractional calculus

1. Introduction

Initial studies about the application of the fractional approach to electromagnetic theory were performed by Engheta in the 1990s [1–3]. He introduced the idea of the fractional paradigm in electromagnetics, which states that there are continuous intermediate stages between two canonical states of the electromagnetic field. Using the properties of the fractional derivative approach, the intermediate stages of fields or sources between two canonical states can be described [1–5]. Since then, several studies have been performed on scattering problems [6–10]. The integral boundary condition, which corresponds to an intermediate boundary condition between Dirichlet and Neumann boundary conditions, is used in order to explain the scattering properties of different geometries. By determining the fractional order (FO), the scattering properties of different materials are investigated. Throughout the study, the integral boundary condition can also be pronounced as the fractional boundary condition (FBC), which was explained in previous studies [7, 8].

The boundary conditions used in previous works [7–9] describe a new material property (perfect electric conductor (PEC), perfect magnetic conductor (PMC), or in between). In these studies, theoretical and numerical results are obtained for the plane wave diffraction by one strip, two strips with the same length, and a semiinfinite strip. In the case of real fractional order, the impedance of the strip is found as a purely imaginary value.

In this paper, a complex fractional order that has both real and imaginary parts is introduced for the first time. The impedance of the strip is found to be complex-valued. Therefore, the fractional boundary condition with the complex fractional order describes a new kind of material with different properties. Several different cases such as different operating frequencies, strip length, and fractional orders are investigated both theoretically and numerically. Then the results are presented.

This paper is organized as follows. In Section 2, the formulation of the problem and the theoretical results are introduced briefly. In Section 3, the convergence study for the numerical analysis is presented. Next, in

*Correspondence: karacuha17@itu.edu.tr

Sections 4 and 5, physical characteristics of the electric field and numerical results are introduced, respectively. Finally, the conclusion of this paper is drawn in Section 6.

2. Formulation of the problem

The main focus of this section is the investigation of E–polarized electromagnetic plane wave diffraction by a strip with the fractional boundary condition (FBC). There is a strip that has width 2a and infinitesimal height. The strip is located at $y = 0$ and has an infinite length in the z–axis. The geometry of the problem is shown in Figure 1. From the definition of the Riemann–Liouville equation [11], the fractional derivative can be found as:

$$D_y^{\nu} f(y) = \frac{1}{\Gamma(1-\nu)} \frac{d}{dy} \int_{-\infty}^{y} \frac{f(t)}{(y-t)^{\nu}} dt. \tag{1}$$

Here, D_y^{ν} stands for the derivative operator and means that the derivative is taken with respect to y in the order of ν. The real part of the fractional order is shown as $Re(\nu)$, which varies within the range of $0 < Re(\nu) < 1$, and $\Gamma(\nu)$ is the gamma function.

After defining the fractional derivative, it is necessary to define the FBC [7–10]. $U(x, y)$ is the function subjected to the FBC at $y = d$, which is the boundary of the strip in a two-dimensional case. For the plane surface boundary S located at $y = d$, the general form of FBC is written as follows:

$$D_y^{\nu} U(x, y)|_{y \epsilon S} = 0, y = \pm d. \tag{2}$$

In electromagnetic problems, U(x,y) becomes $E_z(x, y)$ or $H_z(x, y)$ depending on the polarization. In this problem, the incident wave is E–polarized; therefore, $U(x, y)$ stands for $E_z(x, y)$. The total electric field $\vec{E}_z$ is composed of the superposition of two fields, which are a plane wave as an incidence wave $\vec{E}^i$ and the scattered electric field $\vec{E}_z^s$, respectively. The monochromatic incidence wave can be denoted as

$$\vec{E}_i = \vec{a}_z e^{-ik(x cos\theta + y \sin\theta)}. \tag{3}$$

Here, $\vec{a}_z$ is the unit vector along the z-axis, θ is the angle of incidence, $k = 2\pi/\lambda$ is the wave number, and λ is the wavelength in free space. Note that the time dependency throughout this study is taken as $e^{-i\omega t}$ and then is omitted. The total electric field can be represented as follows:

$$\vec{E}_z = \vec{E}_z^i + \vec{E}_z^s. \tag{4}$$

In order to find the scattered electric field, the total electric field needs to satisfy the boundary condition on the surface of the strip [7–10]. Here, the boundary condition is the fractional boundary condition and the mathematical expression is given as:

$$D_{ky}^{\nu} E_z(x, y)|_{y=\pm 0} = 0. \tag{5}$$

where $x, -a < x < a$.

Here, the derivative is taken with respect to ky, which is a dimensionless parameter, and y is the normal direction on the strip. The boundary condition given in (5) covers both Dirichlet and Neumann type boundary

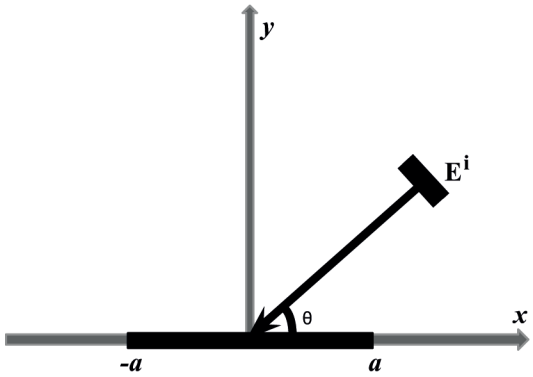

Figure 1. The geometry of the problem.

conditions for $\nu = 0$ and $\nu = 1$, respectively. For fractional order, ν is equal to 0; it corresponds to a PEC surface, whereas for fractional order, ν is equal to 1 and the surface corresponds to a PMC surface. Therefore, the FBC is a more general boundary condition covering both Dirichlet and Neumann type boundary conditions [7–10].

The scattered electric field can be expressed as the convolution of fractional current density induced on the strip and the fractional Green function given as:

$$E_z^s(x,y) = \int_{-\infty}^{\infty} f^{1-\nu}(x')G^{\nu}(x-x',y)dx'. \tag{6}$$

Here, $f^{1-\nu}(x')$ is an unknown function, which is called the fractional current density and has only nonzero values on the strip. The current density has zero values outside of the strip. The fractional Green's function $G^{\nu}(x)$ has the form given as follows [5–7]:

$$G^{\nu}(x-x',y) = -\frac{i}{4}D_{ky}^{\nu}H_0^{(1)}(k\sqrt{(x-x')^2+y^2}), \tag{7}$$

where $H_0^{(1)}$ is the Hankel function of the first kind and zero order. Its spectral representation is given in (8). By the spectral representation, the Hankel function can be written as the summation of plane waves [5–7]:

$$H_0^{(1)}(k\sqrt{(x-x')^2+y^2}) = \frac{1}{\pi}\int_{-\infty}^{\infty} e^{ik[(x-x')\alpha+|y|\sqrt{1-\alpha^2}]}\frac{d\alpha}{\sqrt{1-\alpha^2}}. \tag{8}$$

In order to find the expression for the scattered electric field, (7) is inserted into (6) using (8). Then the scattered electric field is found as in (9). It should be denoted that the fractional derivative of the exponential term is taken as $D_x^{\nu}e^{ikx} = (ik)^{\nu}e^{ikx}$, which is found by using (1) [11, 12]. The reason for denoting the derivative of exponents is that both the incidence and the scattered electric field can be expressed in terms of exponentials

and then the FBC can be applied:

$$E_z^s(x,y) = -i\frac{e^{\pm\frac{i\pi}{2}\nu}}{4\pi}\int_{-\infty}^{\infty} F^{1-\nu}(\alpha)e^{ik[(x\alpha\pm y\sqrt{1-\alpha^2}]}(1-\alpha^2)^{\frac{\nu-1}{2}}d\alpha, \tag{9}$$

where

$$F^{1-\nu}(\alpha) = \textstyle\int_{-1}^{1} \widetilde{f}^{1-\nu}(\xi)e^{-i\epsilon\alpha\xi}d\xi, \qquad \widetilde{f}^{1-\nu}(\xi) = af^{1-\nu}(a\xi),$$

$$\epsilon = ka, \qquad \xi = \tfrac{x}{a}, f^{1-\nu}(\xi) = \tfrac{\epsilon}{2\pi}\textstyle\int_{-\infty}^{\infty} F^{1-\nu}(\alpha)e^{-i\epsilon\alpha\xi}d\alpha\,.$$

The integral representation in (9) satisfies the wave equation and the Sommerfeld radiation condition where the (+) sign stands for the upper half space ($y>0$) and (-) corresponds to the lower half space ($y<0$). After finding the scattered electric field, the FBC is applied to the total electric field as given in (5). Then the integral equation (IE) is obtained as given in (10):

$$\int_{-\infty}^{\infty} F^{1-\nu}(\alpha)e^{i\epsilon x\alpha}\left(1-\alpha^2\right)^{\nu-1/2}d\alpha = -4i\pi e^{-\frac{i\pi\nu}{2}}(\sin\theta)^{\nu}e^{-ikx\cos\theta}. \tag{10}$$

By multiplying the integral equation in (10) by $e^{-ix\epsilon\beta}$ and integrating with respect to x from –a to a, IE (11) is obtained. For any arbitrary fractional order ν, IE (11) needs to be solved in order to find the Fourier transform of the fractional current density:

$$\int_{-\infty}^{\infty} F^{1-\nu}(\alpha)\frac{\sin\varepsilon(\alpha-\beta)}{\alpha-\beta}\left(1-\alpha^2\right)^{\nu-\frac{1}{2}}d\alpha = -4i\pi(\sin\theta)^{\nu}e^{-\frac{i\pi\nu}{2}}(\sin\theta)^{\nu}\frac{\sin\varepsilon(\beta+\cos\theta)}{\beta+\cos\theta}. \tag{11}$$

In order to satisfy Meixner's edge condition [13], a series of Gegenbauer polynomial representations $C_n^{\nu}(\xi)$ for the normalized current density $\widetilde{f}^{1-\nu}$ with the weighting function $(1-\xi)^{\nu-1/2}$ and the unknown ζ_n^{α} are used. The normalized current density can be expressed as in (12):

$$\tilde{f}^{1-\nu}(\xi) = (1-\xi)^{\nu-\frac{1}{2}}\sum_{n=0}^{\infty}\zeta_n^{\nu}\frac{C_n^{\nu}(\xi)}{\nu}. \tag{12}$$

Then the Fourier transform of the current density can be found as in (13) [7–10]:

$$F^{1-\nu}(\alpha) = \frac{2\pi}{\Gamma(\nu+1)}\sum_{n=0}^{\infty}(-i)^n\zeta_n^{\nu}\beta_n^{\nu}\frac{J_{n+\nu}(\varepsilon\alpha)}{(2\varepsilon\alpha)^{\nu}}. \tag{13}$$

Here, $\epsilon = ka$, $J_{n+\nu}(\epsilon\alpha)$ are Bessel functions and $\beta_n^{\nu} = \Gamma(n+2\nu)/\Gamma(n+1)$.

By substituting (13) into (11), the integral equation (11) is converted into the system of linear algebraic equation (SLAE) by introducing the unknown ζ_n^{α}. Note that the properties of discontinuous integrals of Weber-Shafheitlin and (14) are taken into account [14, 15]. The SLAE can be given as in (15):

$$\frac{1}{\pi}\int_{-\infty}^{\infty}\frac{J_{n+\nu}(\varepsilon\alpha)}{\alpha^{\nu}}\frac{\sin(\varepsilon(\alpha-b))}{\alpha-\beta}d\alpha = \frac{J_{n+\nu}(\varepsilon\beta)}{\beta^{\nu}}, \tag{14}$$

$$\sum_{n=0}^{\infty}(-i)^n\zeta_n^{\alpha}\beta_n^{\nu}C_{mn}^{\nu}=\chi_m^{\nu}, \tag{15}$$

where

$$C_{mn}^{\nu}=\int_{-\infty}^{\infty}\mathcal{J}_{n+\nu}(\varepsilon\alpha)\mathcal{J}_{m+\nu}(\varepsilon\alpha)\left(1-\alpha^2\right)^{\nu-\frac{1}{2}}\frac{d\alpha}{\alpha^{2\nu}},$$

$$\chi_m^{\nu}=-2i\Gamma(\nu+1)(-i)^{\nu}(2\varepsilon)^{\nu}(\sin\theta)^{\nu}\frac{J_{m+\nu}(\varepsilon\cos\theta)}{(\cos\theta)^{\nu}}.$$

3. Investigation of convergence in numerical analysis

When FO, ν becomes complex-valued, and the convergence of C_{mn}^{ν} given in (15) is not satisfactory. In order to have better convergence, the manipulation in the integral expression of C_{mn}^{ν} is done. In other words, the integral C_{mn}^{ν} is split into two parts as the first integral from $-\infty$ to 0 and the second integral from 0 to ∞. Then, in the first integral part, a change of variable is applied (q $\rightarrow$ –q). After that, the expression given in (16) is found:

$$C_{mn}^{\nu}=\left[1+(-1)^{m+n}\right]\int_0^{\infty}J_{n+\nu}(\varepsilon q)J_{m+\nu}(\varepsilon q)\frac{\left(1-q^2\right)^{\nu-\frac{1}{2}}}{q^{2\nu}}dq. \tag{16}$$

In order to increase the convergence, the term $(1-q^2)^{\nu-1/2}$ in (16) can be written as (17):

$$\left(1-q^2\right)^{\nu-\frac{1}{2}}=\left(1+(iq)^2\right)^{\nu-\frac{1}{2}}=q^{2\nu-1}\left[-\left(1-\frac{1}{q^2}\right)\right]^{\nu-\frac{1}{2}}. \tag{17}$$

Here, we define $\gamma_\nu(q)$ as $\gamma_\nu(q)=[-(1-\frac{1}{q^2})^{\nu-1/2}]-1$. Then $\gamma_\nu(q)$ is substituted into (16). The corresponding integral would have two parts as $C_{mn}^{1,\nu}$ and $C_{mn}^{2,\nu}$, which are shown in (18):

$$C_{mn}^{\nu}=\left[1+(-1)^{m+n}\right]\int_0^{\infty}J_{n+\nu}(\varepsilon q)J_{m+\nu}(\varepsilon q)\frac{q^{2\nu-1}}{q^{2\nu}}\left[\gamma_\nu(q)+1\right]dq=C_{mn}^{1,\nu}+C_{mn}^{2,\nu}. \tag{18}$$

Here,

$$C_{mn}^{1,\nu}=\left[1+(-1)^{m+n}\right]\int_0^{\infty}J_{n+\nu}(\varepsilon q)J_{m+\nu}(\varepsilon q)\frac{dq}{q},$$

$$C_{mn}^{2,\nu}=\left[1+(-1)^{m+n}\right]\int_0^{\infty}J_{n+\nu}(\varepsilon q)J_{m+\nu}(\varepsilon q)\gamma_\nu(q)\frac{dq}{q}.$$

$C_{mn}^{1,\nu}$ has an analytical solution [14, 15]. The result of the integral $C_{mn}^{1,\nu}$ is given in (19):

$$C_{mn}^{1,\nu}=\left[1+(-1)^{m+n}\right]\frac{2}{\pi(m+n+2\nu)(m-n)}\sin\left(\frac{m-n}{2}\pi\right), \tag{19}$$

where $Re(m+\nu,n+\nu)>0$.

On the other hand, the integral $C_{mn}^{2,\nu}$ is taken numerically. When q goes to infinity (q$\rightarrow\infty$), $C_{mn}^{2,\nu}$ has the same behavior as $O(\frac{1}{q^{2(1+\nu)}})$.

4. Physical characteristics of the electric field

In this section, the total radar cross-section (TRCS) and the relation between the impedance and the fractional order are given. After having the expression for $F^{1-\nu}$ given as in (13), the radiation pattern of the scattered electric field in the far zone can be found using (20). For large values of ka (ka $\rightarrow \infty$), the scattered electric field gets the next form by the stationary phase method [8]. Here, $x = rcos\phi$ and $y = rsin\phi$.

$$E_z^s(x,y) = A(kr)\Phi^\nu(\phi), \tag{20}$$

where $A(kr) = \sqrt{\frac{2}{\pi kr}}e^{ikr-i\frac{\pi}{4}}$ and $\Phi^\nu = -\frac{i}{4}(\pm)^\nu F^{1-\nu}(cos\phi)sin^\nu(\phi)$.

In (20), $\Phi^\nu(\phi)$ is denoted as the radiation pattern (RP). The upper sign in the Φ^ν expression is chosen for $\phi \in [0, \pi]$, and the lower sign stands for $\phi \in [\pi, 2\pi]$, where ϕ is the observation angle. A(kr) corresponds to the radial and $\Phi^\nu(\phi)$ is the angular part of the scattered electric field in the far zone.

Total radar cross-section is another investigation of physical characteristics of the electric field. In order to find TRCS, (21) is taken into account [16]:

$$\sigma_t = \int_0^{2\pi} |\Phi^\nu|^2 \, d\phi. \tag{21}$$

The other important physical characteristic of the strip is the impedance. The normalized impedance of the strip can be found as $\eta_\nu = -\frac{i}{sin\theta}tan(\frac{\pi\nu}{2})$ [7, 9]. Then the fractional order for the specific impedance value of the surface can be found by using (22). Throughout this paper, the impedance, permittivity, and permeability are assumed to be relative values with respect to the vacuum:

$$\nu = \frac{1}{i\pi}\ln\left(\frac{1-\eta_\nu \sin\theta}{1+\eta_\nu \sin\theta}\right). \tag{22}$$

For the normal incidence case, (22) becomes $\nu = \frac{1}{i\pi}\ln(\frac{1-\eta_\nu}{1+\eta_\nu})$ and this yields $\eta_\nu = -i\tan(\frac{\pi}{2}\nu)$. When the fractional order ν is complex-valued as $\nu = \nu_1 + i\nu_2$, where ν_1 and ν_2 are real numbers and the incidence angle is the normal incidence, the real and imaginary parts of the impedance can be found as (23) and (24). Here, the impedance can also be denoted as $\eta_\nu = \eta_1 + i\eta_2$, where η_1 and η_2 are real numbers:

$$\eta_1 = \frac{\tanh\left(\frac{\pi}{2}\nu_2\right) + \tan^2\left(\frac{\pi}{2}\nu_1\right)\tanh\left(\frac{\pi}{2}\nu_2\right)}{1 + \tan^2\left(\frac{\pi}{2}\nu_1\right)\tanh^2\left(\frac{\pi}{2}\nu_2\right)}, \tag{23}$$

$$\eta_2 = -\frac{\tan\left(\frac{\pi}{2}\nu_1\right) - \tan\left(\frac{\pi}{2}\nu_1\right)\tan^2\left(\frac{\pi}{2}\nu_2\right)}{1 + \tan^2\left(\frac{\pi}{2}\nu_1\right)\tanh^2\left(\frac{\pi}{2}\nu_2\right)}. \tag{24}$$

By the definition, the impedance can be expressed with the expression $\eta = \sqrt{\frac{\mu}{\epsilon}}$, where μ stands for the magnetic permeability and ϵ, in general, is called the complex permittivity. The permittivity can be expressed

as $\epsilon = \epsilon' + i\epsilon''$, where ϵ' is the electric permittivity, while ϵ'' characterizes the absorption or the loss [17]. After some mathematical transformations by using 23 and 24, the real and the imaginary parts of the complex permittivity can be found as follows:

$$\epsilon' = \mu \frac{\eta_1^2 - \eta_2^2}{\left(\eta_1^2 - \eta_2^2\right)^2 + 4\eta_1^2\eta_2^2}, \tag{25}$$

$$\epsilon'' = -\mu \frac{2\eta_1\eta_2}{\left(\eta_1^2 - \eta_2^2\right)^2 + 4\eta_1^2\eta_2^2}. \tag{26}$$

5. Numerical analysis and results

In this part, the total radar cross-section (TRCS), the near electric field distribution, the impedance, and the complex permittivity variation with respect to the fractional order are given. Also, the comparison of radiation patterns obtained by the FBC and the impedance boundary condition is done. The value of the TRCS is shown with respect to ka. Note that fractional order ν can be denoted as $\nu = \nu_1 + i\nu_2$, where ν_1 and ν_2 are real numbers. Also, the impedance can be denoted as η_ν and the real and the imaginary parts of the impedance can be written as $\eta_\nu = \eta_1 + i\eta_2$, where η_1 and η_2 are real numbers. In Figure 2, there is a family of graphs in which the TRCSs of different fractional orders with normal incidence are investigated. The lateral straight line in red corresponds to $\log_{10}(TRCS) = 0$. Here, the half width of strip (a) is equal to 1. The real part of fractional order ν_1 is 0.75, and the imaginary part of fractional order ν_2 changes from 0.1 to 0.8 with steps of 0.1. As seen in Figure 2, resonance peaks are observed. By changing the imaginary part of the fractional order, the sharpness of resonances changes. The resonance becomes sharper when the imaginary part, ν_2, is increased up to 0.7.

While having the imaginary part of the fractional order as 0.6, the TRCS is reaching beyond 1.2 on the logarithmic scale ($\log_{10}(TRCS)$), whereas, when the imaginary part of the fractional order is 0.5, the TRCS becomes approximately 0.65 on the logarithm scale. For the imaginary part of the fractional order, which has values from 0.1 to 0.4, the peak values change slowly. On the other hand, when the imaginary part of the fractional order is between 0.4 and 0.7, the peak values are increasing very rapidly. For the imaginary part of fractional order $\nu_2 = 0.7$, the peak value becomes 3.3 on the logarithmic scale. While the imaginary part of the fractional order, ν_2, is equal to 0.8, again the peak value is decreased. The highest peak value is that in the case that ν_2 is equal to 0.7.

Figure 3 corresponds to the real part of impedance η_1 when the real part of fractional order ν_1 is equal to 0.75. In the figure, the imaginary part of fractional order ν_2 changes from 0.1 to 0.8. The impedance has both real and imaginary parts. The maximum value for the real part of the impedance is observed when the imaginary part of fractional order ν_2 is equal to approximately 0.3. Figure 4 corresponds to the complex part of impedance η_ν when ν_1 is equal to 0.75 and ν_2 changes from 0 to 0.8. The complex part of impedance changes the sign when ν_2 is equal to 0.5. Here, the lateral straight line corresponds to the axis where the imaginary part of impedance, η_2, is equal to zero. When $\nu_2 = 0.5$, the impedance has only the real part. In both Figure 3 and Figure 4, the incidence wave is the normal incidence and the real part of fractional order, ν_1, has the value of 0.75, which is close to the perfect magnetic conductor case.

In Figure 5, there is a family of graphs in which TRCSs of different fractional orders with normal incidence are investigated. Here, the half width of strip (a) is again equal to 1. In this case, the real part of fractional

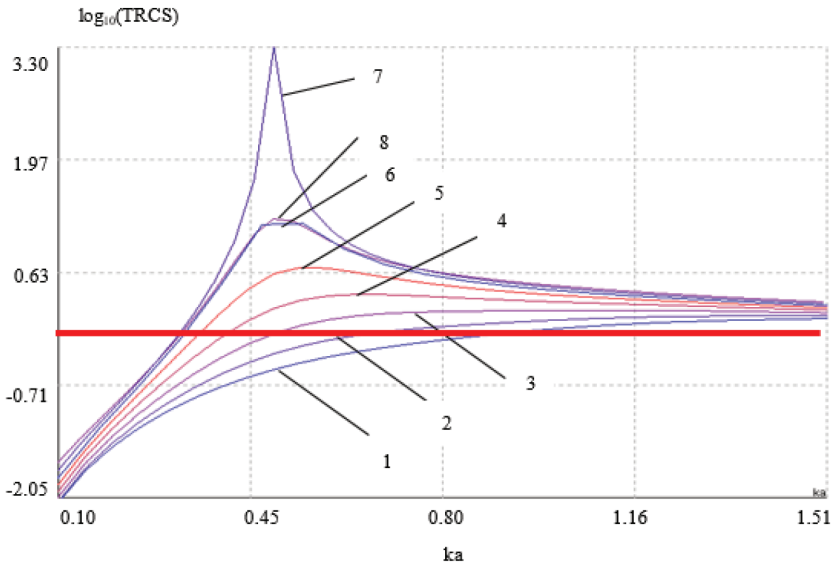

Figure 2. TRCS for 1. $\nu = 0.75 + i0.1$, 2. $\nu = 0.75 + i0.2$, 3. $\nu = 0.75 + i0.3$, 4. $\nu = 0.75 + i0.4$, 5. $\nu = 0.75 + i0.5$, 6. $\nu = 0.75 + i0.6$, 7. $\nu = 0.75 + i0.7$, 8. $\nu = 0.75 + i0.8$, $a = 1$, $\theta = \pi/2$.

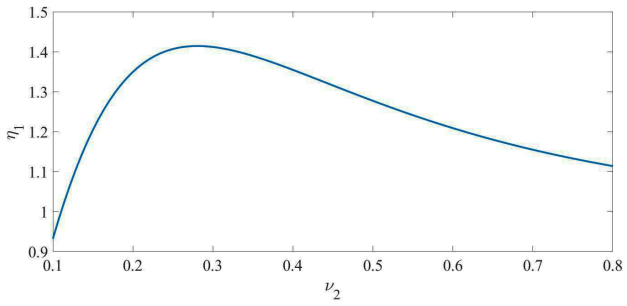

Figure 3. The dependency of the impedance's real part on the imaginary part of fractional order when the real part of fractional order, ν_1, is equal to 0.75.

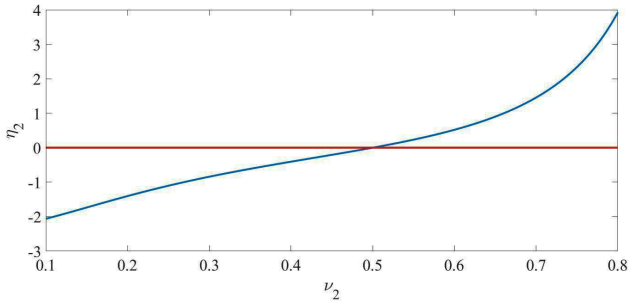

Figure 4. The dependency of the impedance's imaginary part on the imaginary part of fractional order when the real part of fractional order, ν_1, is equal to 0.75.

order ν_1 is 0.2, and the imaginary part of fractional order ν_2 changes from 0.3 to 0.5 with steps of 0.1. As seen in Figure 5, resonance peaks are observed. By changing the imaginary part of the fractional order, the sharpness of resonances changes. When the imaginary part of the fractional order is between 0.3 and 0.4, the peak values change slowly. On the other hand, the peak values are increasing very rapidly and the peaks have higher values when the imaginary part of the fractional order is between 0.4 and 0.6. As seen in Figure 5, the maximum peak value becomes 3.64 when the imaginary part of fractional order, ν_2, is equal to 0.6. Then the peak value decreases again when the imaginary part of fractional order, ν_2, is higher than 0.6.

Figure 6 shows the relation between the real part of impedance η_1 and the imaginary part of fractional order, ν_2, when the real part of fractional order, ν_1 is equal to 0.2. In the figure, the imaginary part of fractional order, ν_2, changes from 0.1 to 0.7. In this case, on the contrary to the previous case given in Figure 3, there is no local maximum. Figure 7 corresponds to the complex part of impedance η_ν when ν_1 is equal to 0.2 and ν_2 changes from 0.1 to 0.7. As we see, the complex part of the impedance changes the sign when ν_2 is equal

to 0.5. The lateral straight red line corresponds to the axis where the imaginary part of the impedance η_2 is equal to zero. In both Figure 6 and Figure 7, the incidence wave is the normal incidence and the real part of fractional order ν_1 is 0.2, which is close to the perfect electric conductor.

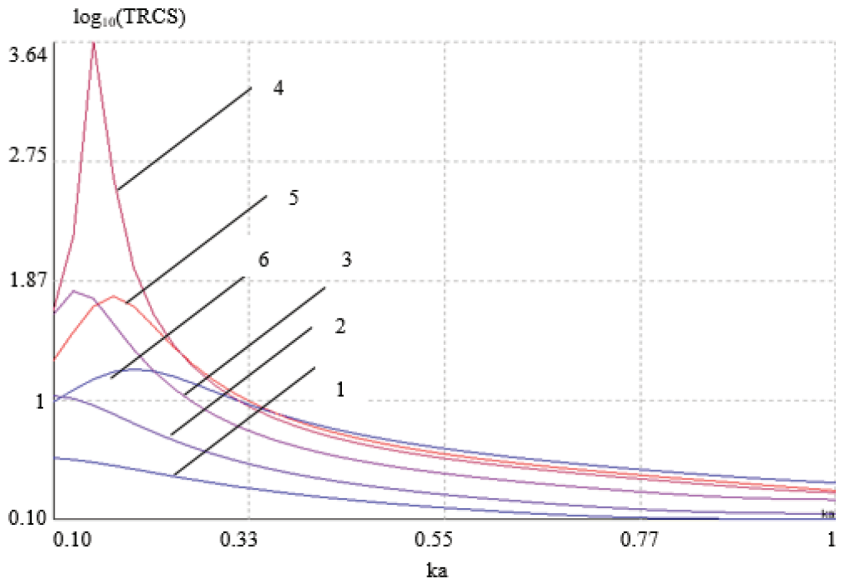

Figure 5. TRCS for 1. $\nu = 0.2 + i0.3$, 2. $\nu = 0.2 + i0.4$, 3. $\nu = 0.2 + i0.5$, 4. $\nu = 0.2 + i0.6$, 5. $\nu = 0.2 + i0.7$, 6. $\nu = 0.2 + i0.8$, $a = 1$, $\theta = \pi/2$.

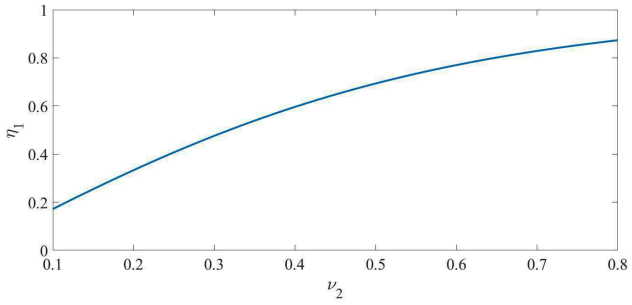

Figure 6. The dependency of the impedance's real part on the imaginary part of fractional order when the real part of fractional order ν_1 is equal to 0.2.

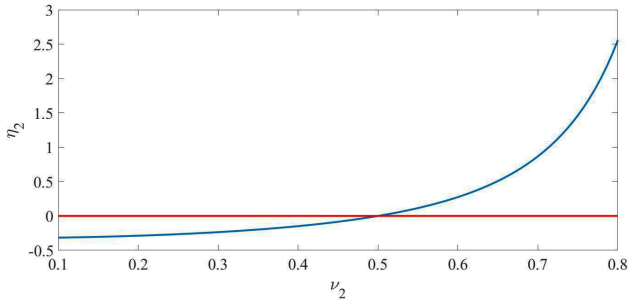

Figure 7. The dependency of the impedance's imaginary part on the imaginary part of fractional order when the real part of fractional order ν_1 is equal to 0.2.

In Figure 8, there is again a family of graphs in which the TRCSs of different fractional orders with normal incidence are studied. Here, the half width of strip (a) is equal to 1. The real part of fractional order ν_1 is equal to 0.5, and the imaginary part of fractional order ν_2 changes from 0.1 to 0.5 with steps of 0.1. As seen in Figure 8, resonance peaks are observed. The values of resonances change with the imaginary part of the fractional order. The resonance becomes sharper when the imaginary part is increased up to 0.7. When the imaginary part is equal to 0.5, the TRCS is reaching beyond 0.72 on the logarithmic scale. TRCS becomes approximately 0.35 on the logarithmic scale when the imaginary part of the fractional order is 0.4. For the imaginary part of the fractional order, which is between 0.1 and 0.4, the peak values change slowly. On the other hand, the peak values are increasing very rapidly in the case of having the imaginary part of the fractional

order that has values between 0.4 and 0.7. Note that the imaginary part of fractional order ν_2 has a value of 0.8, and again the peak value is decreased. Therefore, the highest peak value is seen in the case that ν_2 is equal to 0.7.

Figure 9 investigates the relation between the real part of impedance η_1 and the imaginary part of fractional order ν_2 when the real part of fractional order ν_1 is equal to 0.5. In this case, on the contrary to the previous case given in Figure 3, there is no local maximum. Figure 10 corresponds to the complex part of impedance η_ν when ν_1 is 0.5. Here, ν_2 changes from 0.1 to 0.8 and the complex part of the impedance changes the sign when ν_2 is equal to 0.5. The lateral straight line in Figure 10 corresponds to the axis where the imaginary part of impedance η_2 is equal to zero. When ν_2 is equal to 0.5, the impedance has only the real part. In both Figure 9 and Figure 10, the incidence wave is the normal incidence and the real part of fractional order ν_1 is 0.5, which is exactly the middle of the perfect electric conductor and the perfect magnetic conductor case.

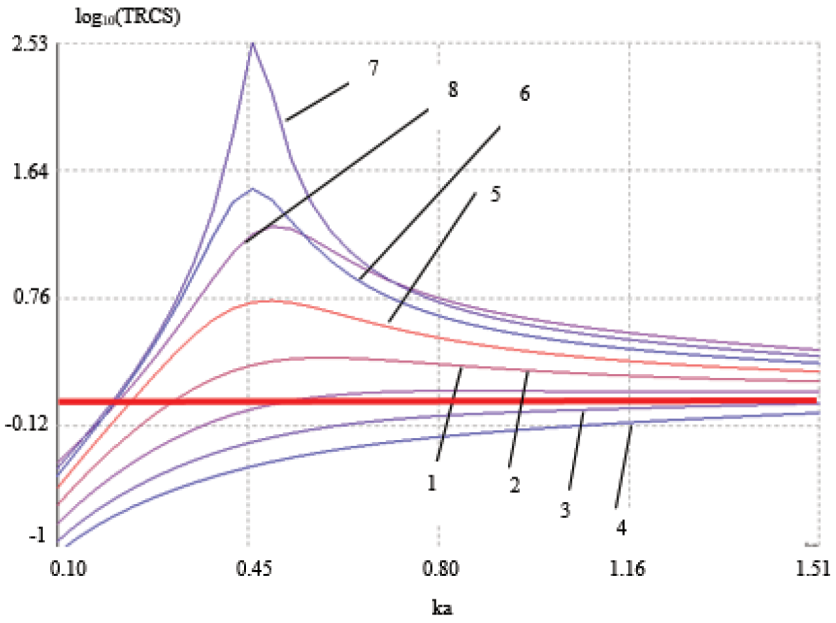

Figure 8. TRCS for 1. $\nu = 0.5 + i0.1$, 2. $\nu = 0.5 + i0.2$, 3. $\nu = 0.5 + i0.3$, 4. $\nu = 0.5 + i0.4$, 5. $\nu = 0.5 + i0.5$, 6. $\nu = 0.5 + i0.6$, 7. $\nu = 0.5 + i0.7$, 8. $\nu = 0.5 + i0.8$, $a = 1$, $\theta = \pi/2$.

In Figures 11–16, the distributions of the total electric field are given. As can be seen in Figure 11, the scattered electric field dominates the total electric field distribution, which is symmetric with respect to the y-axis where the strip is located. In Figure 2, the TRCS gives the resonance ka value of the strip with parameters given as $\nu = 0.75 + i0.7$, $a = 1$, $\theta = \pi/2$. As can be seen in Figure 13, in the resonance case (ka=0.495) found in Figure 2, the near field distribution has a peak value of approximately 40. This is the maximum value of the E–field amplitude for given parameters. In Figure 12, the near field distribution of the total electric field is given for parameters listed as ka $= 0.5$, $\nu = 0.75 + i0.6$, $a = 1$, and $\theta = \pi/2$. In this case, the incidence wave dominates and the peak value is approximately reaching up to 4.25. When Figure 11 and Figure 12 are compared, it can be understood that the complex part of the fractional order affects the distribution of the E–field in the region abruptly.

In Figure 13, again, the near field distribution of the total electric field is given. In the same figure, the

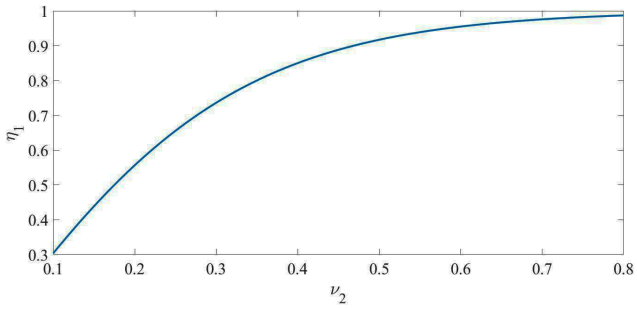

Figure 9. The dependency of the impedance's real part on the imaginary part of fractional order when the real part of fractional order ν_1 is equal to 0.5.

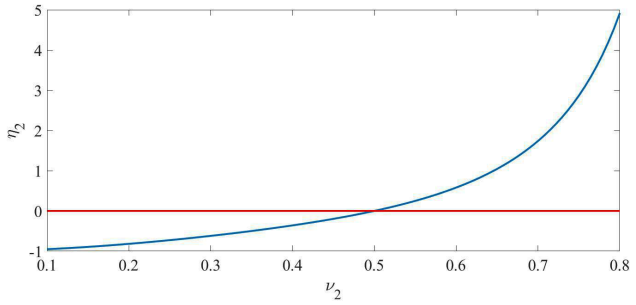

Figure 10. The dependency of the impedance's imaginary part on the imaginary part of fractional order when the real part of fractional order ν_1 is equal to 0.5.

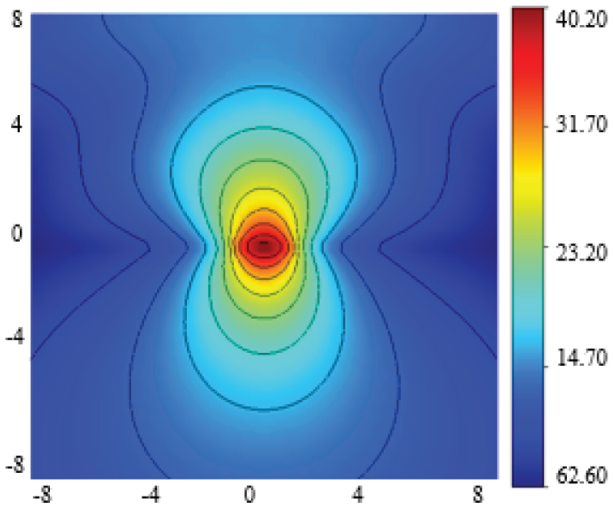

Figure 11. The near field distribution of total electric field at the resonant frequency for $ka = 0.495$, $\nu = 0.75 + i0.7$, $a = 1$, $\theta = \frac{\pi}{2}$.

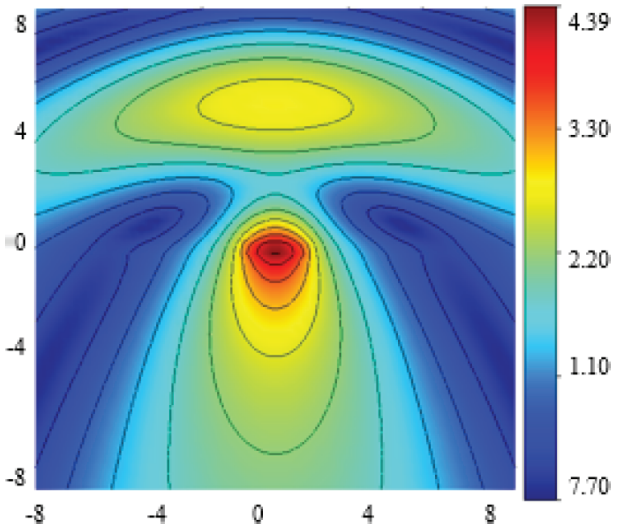

Figure 12. The near field distribution of total electric field at the resonant frequency for $ka = 0.5$, $\nu = 0.75 + i0.6$, $a = 1$, $\theta = \frac{\pi}{2}$.

scattered electric field dominates the incidence field. The field distribution is symmetric with respect to the y-axis where the strip is located. In Figure 5, the TRCS gives the resonance ka value of the strip with parameters as $\nu = 0.2 + i0.6$, $a = 1$, $\theta = \pi/2$. As can be seen in Figure 13, in the resonance case (ka=0.146) found in Figure 5, the near field distribution has a peak value of 66. This is the maximum value of the E–field amplitude for given parameters. In Figure 14, the near field distribution of the total electric field is shown. Here the variables are listed as ka=0.169, $\nu = 0.2 + i0.7$, $a = 1$, and $\theta = \pi/2$. In this case, the incidence wave dominates and the peak value is approximately reaching up to 3.21. When Figure 13 and Figure 14 are compared, it can be understood that the complex part of the fractional order dramatically affects the distribution of the E–field in the region.

In Figure 15, similarly, the near field distribution of the total electric field is illustrated. In the same figure, the scattered electric field dominates with respect to the incidence field. The field distribution is not symmetric completely with respect to the y-axis where the strip is located because, in this case, the ka value is not the same as the resonance value, but still, the scattering field dominates. As can be seen in Figure 15, the

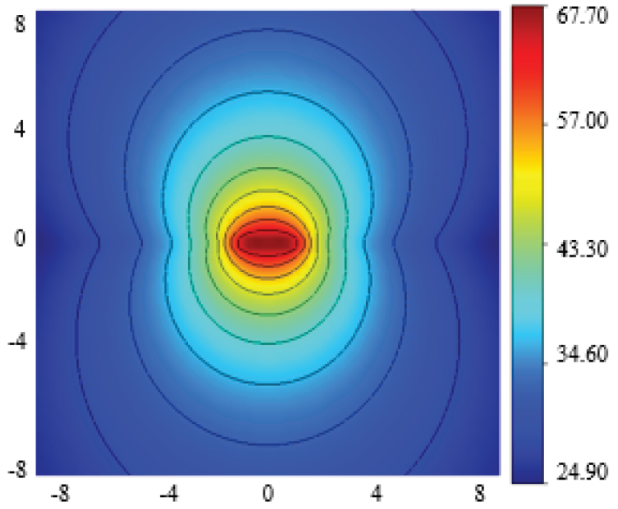

Figure 13. The near field distribution of total electric field at the resonant frequency for $ka = 0.146$, $\nu = 0.2 + i0.6$, $a = 1$, $\theta = \frac{\pi}{2}$.

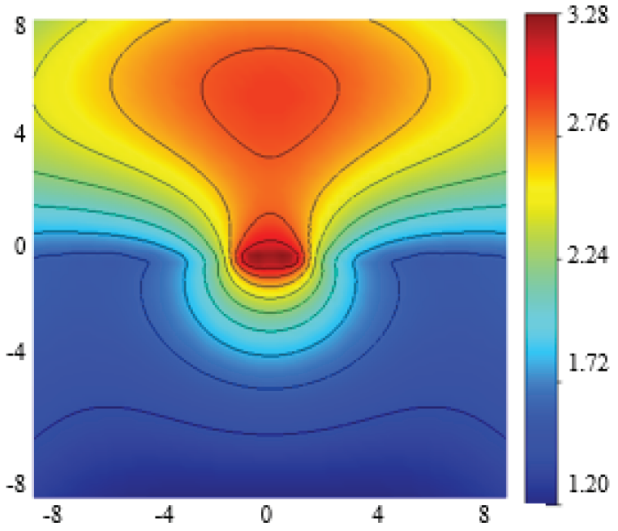

Figure 14. The near field distribution of total electric field at the resonant frequency for $ka = 0.169$, $\nu = 0.2 + i0.7$, $a = 1$, $\theta = \frac{\pi}{2}$.

near field distribution has a peak value of approximately 13.5 when ka is chosen near the resonance value. In Figure 16, for parameters given as ka = 0.331, $\nu = 0.5 + i0.6$, $a = 1$, and $\theta = \pi/2$, the near field distribution of the total electric field is given. In this case, the incidence wave dominates and the peak value is approximately reaching up to 4.51. When Figure 15 and Figure 16 are compared, again, it can be understood that the complex part of the fractional order plays an important role in the distribution of the E–field in the region.

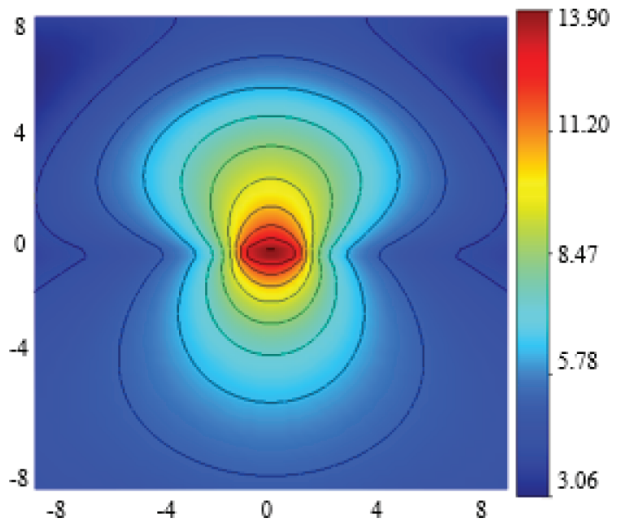

Figure 15. The near field distribution of total electric field for $ka = 0.331$, $\nu = 0.5 + i0.7$, $a = 1$, $\theta = \frac{\pi}{2}$.

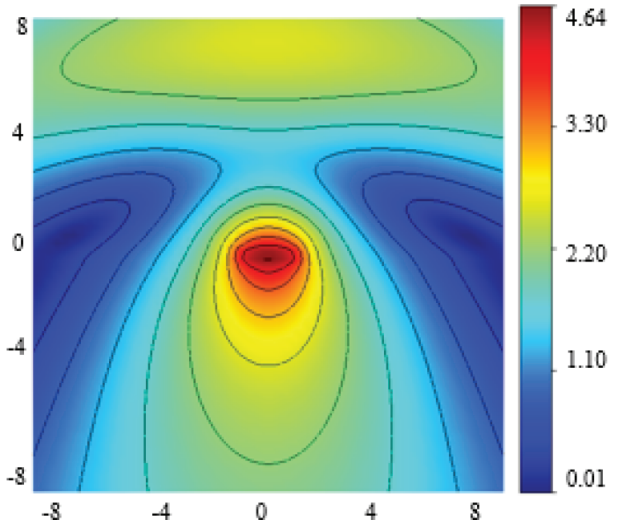

Figure 16. The near field distribution of total electric field near for $ka = 0.331$, $\nu = 0.5 + i0.6$, $a = 1$, $\theta = \frac{\pi}{2}$.

In Figure 17 and Figure 18, in order to verify the fractional derivative method (FDM), the comparisons of radiation pattern $\Phi^{\nu}(\phi)$ are done between the results obtained by the fractional boundary condition

and impedance boundary condition (IBC) for two different values of the fractional order and corresponding impedance values ($\phi \in [0, \pi]$) [9]. For the fractional order $\nu = 0.5 + i0.5$, the corresponding impedance value becomes $\eta = 0.9172$, and for the fractional order $\nu = 0.75 + i0.7$, the corresponding impedance value becomes $\eta = 1.1546 + i1.4546$ as found by (23) and (24).

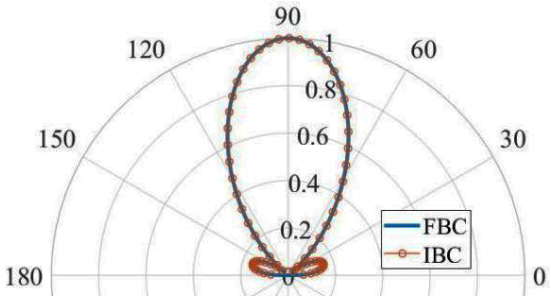

Figure 17. Comparison of radiation pattern for normal incidence between the fractional boundary condition (FBC) and the impedance boundary condition (IBC) for $\nu = 0.5 + i0.5$.

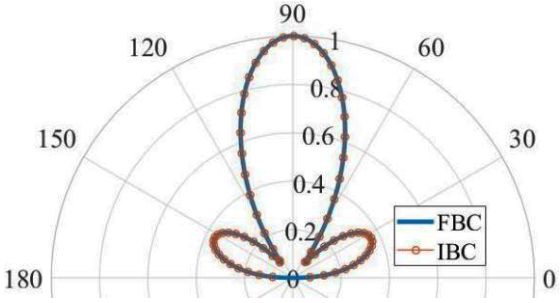

Figure 18. Comparison of radiation pattern for normal incidence between fractional boundary condition (FBC) and impedance boundary condition (IBC) for $\nu = 0.75 + i0.7$.

Figure 19 shows a graph on which the real part of the complex permittivity ϵ' changes when the imaginary part of the complex fractional order changes in the range of $0.1 < \nu_2 < 0.8$ while ν_1 is 0.75. There are the maximum and the minimum values in the range. Figure 20 shows the relation between the imaginary part of the complex permittivity ϵ'' on the imaginary part of the complex fractional order when it changes in the range of $0.1 < \nu_2 < 0.8$. When ν_2 is 0.6, the graph has a minimum. Besides, in the range of $0.5 < \nu_2 < 0.8$, ϵ'' is negative-valued. This means that the strip with corresponding parameters has "negative absorption" [17]. This explains why there are peak values in Figure 2. As can be seen in Figure 2, after the complex part of the fractional order ν_2 reaches 0.5, TRCS values are increasing sharply for the specific ka values because the complex part of the permittivity becomes negative for this range as given in Figure 20. When the complex part of the fractional order ν_2 becomes 0.7, the TRCS has the maximum value. After that, the resonance values are decreasing for increasing values of the complex part of the fractional order ν_2 because, for this case, the complex part of the permittivity is again closing to the zero value. In other words, when the complex part of the permittivity ϵ'' is getting negative minimum values, the resonance values increase because the negative absorption property of the material is increasing as seen in Figure 20.

6. Conclusion

In this article, the plane electromagnetic wave diffraction was considered by the strip. The two-dimensional problem was solved when the strip is infinite in z-direction. As the boundary condition, the fractional boundary condition with complex-valued fractional order is required on the surface of the strip. The complex-valued fractional order gave interesting results. In the results, a new type of resonance is observed, and its property was studied using the TRCS and the near field distribution. This resonance does not exist for real fractional order. Therefore, this is a unique property of the complex-valued fractional order boundary condition. The corresponding impedance value of the strip was also demonstrated.

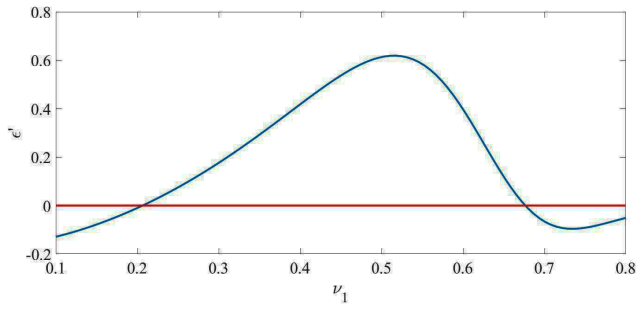

Figure 19. The dependency of the permittivity's real part on the imaginary part of the fractional order when the real part of the fractional order ν_1 is 0.75.

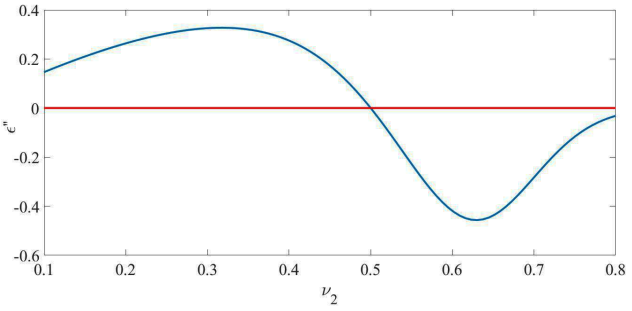

Figure 20. The dependency of the permittivity's imaginary part on the imaginary part of the fractional order when the real part of the fractional order ν_1 is 0.75.

Acknowledgment

We would like to thank Damla Alptekin, Prof. Dr. Ertuğrul Karaçuha, and Prof. Dr. Nader Engheta for their contributions to the subject.

References

[1] Engheta N. Use of fractional integration to propose some "fractional" solutions for the scalar Helmholtz equation. Progress in Electromagnetics Research 1996; 12: 107-132.

[2] Engheta N. Fractional curl operator in electromagnetics. Microwave and Optical Technology Letters 1998; 17 (2): 86-91.

[3] Engheta N. Phase and amplitude of fractional-order intermediate wave. Microwave and Optical Technology Letters 1999; 21(5): 338-343.

[4] Engheta N. Fractionalization methods and their applications to radiation and scattering problems. In: IEEE International Conference on Mathematical Methods in Electromagnetic Theory; Ukraine; 2000. pp. 34-40. doi: 10.1109/MMET.2000.888504

[5] Veliev EI, Engheta N. Generalization of Green's theorem with fractional differintegration. In: IEEE AP-S International Symposium and USNC/URSI National Radio Science Meeting; Ohio, USA; 2003. p. 228.

[6] Ivakhnychenko MV, Veliev EI. Fractional curl operator in radiation problems. In: 10th IEEE International Conference on Mathematical Methods in Electromagnetic Theory; Ukraine; 2004. pp. 231-233. doi 10.1109/MMET.2004.1396991

[7] Veliev EI, Ahmedov TM, Ivakhnychenko MV. Fractional operators approach and fractional boundary conditions. In: Zhurbenko V (editor). Electromagnetic Waves. Rijeka, Croatia: InTech Open, 2011. doi: 10.5772/16300

[8] Veliev EI, Ivakhnychenko MV, Ahmedov TM. Fractional boundary conditions in plane waves diffraction on a strip. Progress in Electromagnetics Research 2008; 79: 443-462. doi: 10.2528/PIER07102406

[9] Ivakhnychenko MV, Veliev EI, Ahmedov TM. Scattering properties of the strip with fractional boundary conditions and comparison with the impedance strip. Progress in Electromagnetics Research 2008; 2: 189-205. doi: 10.2528/PIERC08031502

[10] Veliyev EI, Karaçuha K, Karaçuha E, Dur O. The use of the fractional derivatives approach to solve the problem of diffraction of a cylindrical wave on an impedance strip. Progress in Electromagnetics Research 2018; 77: 19-25.

[11] Samko SG, Kilbas AA, Marichev OI. Fractional Integrals and Derivatives: Theory and Applications. London, UK: CRC Press, 1993.

[12] Oldham K, Spanier J. The Fractional Calculus Theory and Applications of Differentiation and Integration to Arbitrary Order. New York, NY, USA: Elsevier, 1974.

[13] Hönl H, Maue AW, Westpfahl K. Theorie der Beugung. Berlin, Germany: Springer-Verlag, 1987 (in German).

[14] Bateman H. Higher Transcendental Functions. New York, NY, USA: McGraw-Hill Book Company, 1953.

[15] Prudnikov AP. Integral and Series. New York, NY, USA: Gordon and Breach, 1986.

[16] Ishimaru A. Electromagnetic Wave Propagation, Radiation, and Scattering: From Fundamentals to Applications. Hoboken, NJ, USA: John Wiley and Sons, 2017.

[17] Ji Y, Zhi J, Meihuan Y, Ying Q, Yufeng P. Negative absorption peaks in ultraviolet–visible spectrum of water. ChemistrySelect 2016; 1 (3): 3443-3448.